

MRI mediated, non-invasive tracking of intratumoral distribution of nanocarriers in rat glioma

Efstathios Karathanasis¹, Jaekeun Park^{1,2}, Abhiruchi Agarwal¹,
Vijal Patel¹, Fuqiang Zhao^{1,2}, Ananth V Annapragada³,
Xiaoping Hu^{1,2} and Ravi V Bellamkonda^{1,4}

¹ Wallace H Coulter Department of Biomedical Engineering, Georgia Institute of Technology and Emory University, 313 Ferst Drive, Atlanta, GA 30332, USA

² Biomedical Imaging Technology Center, School of Medicine, Emory University, 531 Asbury Circle, Atlanta, GA 30322, USA

³ School of Health Information Sciences, University of Texas Health Science Center, 7000 Fannin Street, Houston, TX 77030, USA

E-mail: ravi@gatech.edu

Received 28 March 2008, in final form 26 May 2008

Published 17 June 2008

Online at stacks.iop.org/Nano/19/315101

Abstract

Nanocarrier mediated therapy of gliomas has shown promise. The success of systemic nanocarrier-based chemotherapy is critically dependent on the so-called leaky vasculature to permit drug extravasation across the blood–brain barrier. Yet, the extent of vascular permeability in individual tumors varies widely, resulting in a correspondingly wide range of responses to the therapy. However, there exist no tools currently for rationally determining whether tumor blood vessels are amenable to nanocarrier mediated therapy in an individualized, patient specific manner today. To address this need for brain tumor therapy, we have developed a multifunctional 100 nm scale liposomal agent encapsulating a gadolinium-based contrast agent for contrast-enhanced magnetic resonance imaging with prolonged blood circulation. Using a 9.4 T MRI system, we were able to track the intratumoral distribution of the gadolinium-loaded nanocarrier in a rat glioma model for a period of three days due to improved magnetic properties of the contrast agent being packaged in a nanocarrier. Such a nanocarrier provides a tool for non-invasively assessing the suitability of tumors for nanocarrier mediated therapy and then optimizing the treatment protocol for each individual tumor. Additionally, the ability to image the tumor in high resolution can potentially constitute a surgical planning tool for tumor resection.

1. Introduction

Current approaches for the treatment of glioma are limited in their effectiveness because malignant brain tumors are characteristically diffuse, highly invasive, and non-localized (Black and Pikul 1999). Complete surgical resection of malignant gliomas is a rarity, partly due to the inability to clearly map the tumor, and partly because of its invasive nature. Therefore, clinical standard of care includes radiation

therapy and systemic and topical chemotherapy after surgical resection. Unfortunately, radiation and topical delivery of chemotherapeutics using polymer wafers have poor results and extend the median survival by 2–9 months and systemic chemotherapy has been minimally effective (Barker *et al* 1998, Fine *et al* 1993). Given the diffuse and invasive nature of gliomas, the success of systemic chemotherapy is critically dependent on the so-called leaky vasculature to permit drug extravasation across the blood–brain barrier (BBB). Currently, systemic chemotherapy is not the primary treatment of choice for malignant brain tumors due to the exposure of non-target organs to chemotherapeutic resulting

⁴ Address for correspondence: Department of Biomedical Engineering, Georgia Institute of Technology/Emory University, 3108 UA Whitaker Building, 313 Ferst Drive, Atlanta, GA 30332, USA.

from systemic administration and due to the presence of the highly impermeable BBB, which limits transport to lipophilic or low molecular weight, uncharged compounds. Therefore, new strategies improving systemic delivery of chemotherapeutics will be a potent tool for treatment of gliomas.

Nanocarrier mediated therapy of gliomas has shown promise because multifunctional nanocarriers can (i) carry large payloads of one or more types of drugs for therapy or contrast agents for imaging or combos of drugs and contrast agents, and (ii) manipulate pharmacokinetics and biodistribution of systemically-administered agents to increase accumulation in tumor site. This multifunctionality of nanoscale systems is projected to enable personalized cancer therapy by diagnosing, treating, and monitoring the progress of treatment for each individual cancer (Service 2005, van de Wiele *et al* 2002, Koning and Krijger 2007, Torchilin 2006, Mitra *et al* 2006). Such nanocarriers can theoretically be designed not only to carry a range of chemotherapeutic or anti-invasive agents (not just low molecular weight, uncharged lipophilic drugs), but also to both passively and actively target intracranial tumors such as gliomas. Passive targeting results from prolonged circulation of nanocarriers allowing for accumulation at sites with abnormal, leaky vasculature. In recent rodent studies of glioma, effective passive tumor dosing was achieved by intravenous (IV) injections of drug-loaded liposomal nanocarriers (Arnold *et al* 2005). It was demonstrated in patients with glioblastomas and metastatic brain tumors that long-circulating liposomal nanocarriers overcome the BBB in the tumor lesions resulting in 13–19 times higher accumulation in the glioblastoma as compared to the normal brain (Koukourakis *et al* 2000). In addition, active targeting can be achieved by decorating nanocarriers with multiple ligands to increase targeting affinity and selectivity by binding to multiple receptors of the same or different type on cancer cells (Saul *et al* 2006, Hong *et al* 2007).

The success of passive (and subsequent active) targeting of nanoscale chemotherapeutic agent therapy for intracranial tumors is critically dependent on the access that these agents have to tumors via the leaky vasculature across the BBB (Jain 1994, 2001, Maeda *et al* 2000). Unfortunately, it is well known that the degree of tumor vascular leakiness differs not only among same type tumors but even spatially within the same tumor (Fukumura and Jain 2007, Hobbs *et al* 1998, Yuan *et al* 1996). For instance, previous studies in our laboratory showed that the standard deviation of the intratumoral accumulation of liposomal doxorubicin in a rat brain tumor was 150% of the mean value (McNeeley *et al* 2007). However, there exist no tools currently to rationally determine whether tumor blood vessels are amenable to nanocarrier mediated therapy in an individualized, patient specific manner today. Such a determination would no doubt be of great benefit for the planning and assessment of multiple chemotherapeutic strategies. One recent example demonstrating the critical role that tumor vessels play in determining therapeutic outcomes comes from the work of Jain *et al*, where they demonstrate the modulation of tumor vessels by normalizing them leads to better chemotherapeutic outcomes (Jain 2005).

Here, we report the development of a multifunctional long-circulating nanocarrier trackable by magnetic resonance imaging (MRI). The nanocarrier consists of a 100 nm scale Pegylated liposomal carrier encapsulating Gadolinium (Gd) and/or a chemotherapeutics. Conventional MR contrast agents, such as Gd chelates, restrict the time window for image acquisition due to their rapid elimination from blood. In the recent past, we demonstrated that the prolonged blood circulation of the agent allowed enhanced signal for long scanning times resulting in high resolution MR images of rat vasculature (Ayyagari *et al* 2006). Other groups have also utilized Gd-loaded liposomal formulations as a paramagnetic agent for angiography resulting in a positive signal enhancement associated with T_1 -shortening (Ghaghada *et al* 2007, Erdogan *et al* 2008, 2006, Torchilin 1994, Krauze *et al* 2006, Weissing *et al* 2000). In this work, we have validated the utility of the Gd-nanocarrier for non-invasive determination of tumor vasculature permeability to nanoparticles in 9L glioma model rat using a 9.4 T Bruker Biospin MR system. Interestingly, under this strength of the magnetic field, the Gd-containing nanocarrier produces negative signal enhancement due to significant T_2 shortening resulting in a more potent contrast agent. While more intricate nanoparticle systems are novel from a materials science perspective, their potential for translation to clinical use is limited by the dearth of knowledge about their toxicity, biodistribution and *in vivo* fate, while liposomal nanoparticles are relatively well characterized and thus provide the potential for rapid translation to the clinic. For instance, nanoscale liposomal doxorubicin formulations were the first nanotherapeutics to be approved for clinical use as the first line for treatment of AIDS-related Kaposi's Sarcoma and relapsed ovarian cancer (Lasic and Papahadjopoulos 1995) and is under numerous clinical trials (128 active studies) for treatment of many types of cancer (www.ClinicalTrials.gov; accessed 12/12/2007). Besides liposomal doxorubicin, other liposomal formulations (Ferrari 2005), polymeric micelles and polymer-based particles (Heath and Davis 2007, Schifflers *et al* 2004, Kim and Rossi 2007) are under preclinical and clinical evaluation.

2. Materials and methods

2.1. Materials

The phospholipids 1,2-dipalmitoyl-sn-glycero-3-phosphocholine (DPPC) and 1,2 disteoyl-sn-glycero-phosphoethanolamine poly(ethylene glycol)₂₀₀₀ (DSPE-PEG₂₀₀₀) were purchased from Genzyme Pharmaceuticals (Cambridge, MA). Cholesterol was purchased from Sigma (St Louis, MO). Gado-diamide (Omniscan) was obtained from GE Healthcare (Milwaukee, WI). 1,2-Dipalmitoyl-sn-glycero-phosphoethanolamine-*N*-(lissamine rhodamine B sulfonyl) (DPPE-lissamine-rhodamine) was purchased from Avanti Lipids (Birmingham, AL). Mouse monoclonal anti-rat CD31 antibody was obtained from BD Biosciences Pharmingen (San Diego, CA). The mouse anti-rat RECA-1 monoclonal antibody (IgG1) was purchased from GeneTex (San Antonio, TX). The secondary antibodies, Alexa Fluor 594

goat anti-rabbit IgG and Alexa Fluor 488 goat anti-mouse, and 2-(3-(diphenylhexatrienyl)propanoyl)-1-hexadecanoyl-*sn*-glycero-3-phosphocholine (β -DPH-HPC) were purchased from Invitrogen (Carlsbad, CA). All animals were purchased from Harlan (Indianapolis, IN). A 9L glioma cell line was received as a generous donation from the Neurosurgery Tissue Bank at UCSF. Minimal essential medium containing Earle's balanced salt solution (MEM/EBSS) was purchased from Hyclone (Logan, UT). Gentamicin (50 mg ml⁻¹), fetal bovine serum (FBS), and Leibovitz's L-15 medium were obtained from Gibco (Carlsbad, CA). Trypsin-EDTA (0.05% trypsin, 0.53 mM EDTA) in Hanks' balanced salt solution was purchased from Mediatech (Herndon, VA). Heparin and isoflurane were obtained from Baxter Healthcare (Deerfield, IL). Ketamine was purchased from Fort Dodge Laboratories (Madison, NJ). Marcaine was obtained from Abbott Laboratories (Abbott Park, IL). Flunixin meglumine was purchased from Phoenix Scientific (San Marcos, CA). Xylazine was purchased from The Butler Company (Dublin, OH). Acetylpromazine (10 mg ml⁻¹) was obtained from Boehringer Ingelheim (Ingelheim, Germany). The rest of the reagents were of analytical grade (Fisher Scientific, Atlanta, GA).

2.2. Fabrication and characterization of the Gd-nanocarrier

A lipid composition of DPPC, cholesterol and DSPE-PEG₂₀₀₀ in the molar ratio of 55:40:5 was used. Fluorescent phospholipid (β -DPH-HPC) at 0.01 mol% was used to track phospholipid content. The formulations used in the *in vivo* imaging studies were tagged with DPPE-Lissamine-Rhodamine at 1 mol% of the total lipids (for fluorescent microscopy of tissue sections as described in section 2.8). The lipids were dissolved in ethanol and hydrated with 0.5 M gadodiamide (Gd) solution at 60 °C followed by sequential extrusion in a Lipex Biomembranes Extruder (Northern Lipids, Vancouver, Canada), to size the liposomal nanocarrier to about 100 nm. Free, un-encapsulated gadodiamide was replaced by a saline solution (300 mM NaCl; 596 mOsm kg⁻¹ water) with comparable osmolarity as the internal phase of the nanocarrier using a 2-day dialysis with a 100k molecular weight cutoff dialysis tubing. The size of the Gd-nanocarrier was determined by dynamic light scattering (90 Plus Particle Size Analyzer, Brookhaven Instruments, Holtsville, NY). The osmolality of the nanocarrier was determined using a vapor osmometer (Wescor, Logan, UT).

2.3. *In vitro* T₁ and T₂ measurements

In vitro, the spin-lattice T₁ and spin-spin T₂ relaxation times of the Gd-nanocarrier suspension and gadodiamide solution were determined on a 0.47 T Bruker Minispec NMR system at 37 °C. The longitudinal and transverse relaxation rates were determined by an inversion recovery pulse sequence and a spin-echo sequence, respectively. To determine the effective Gd concentration, the liposomal nanocarrier was lysed with 20% SDS (sodium dodecyl sulfate). The effective relaxivity (per unit Gd concentration) in the nanocarrier was then determined from the equation: $r_1 = (T_{1\text{Gd}}^{-1} - T_{1\text{noGd}}^{-1})/[\text{Gd}]$; where T_{1Gd}

(or T_{2Gd}) is the observed T₁ (or T₂) relaxation time for the Gd-containing formulations, T_{1noGd} (or T_{2noGd}) is the observed T₁ (or T₂) relaxation time for the buffer, and r₁ (or r₂) is the relaxivity of gadodiamide at 37 °C. T₁ and T₂ relaxation times of the formulations were measured over a concentration range of 0.5–2.0 mM Gd. The r₁ (and r₂) relaxivity were then determined from the slope of the linear regression fits of 1/T₁ (and 1/T₂) against the Gd concentration.

Comparative T₁ and T₂ measurement at 9.4 T were performed on a Bruker Biospin MR system. A series of fast imaging in steady-state precession (TrueFISP) sequences was performed for T₁ measurements. The parameters for the TrueFISP were TR/TE = 3 ms/1.5 ms, delay time = 8 s. A total of 40 frames were acquired during one excitation with inversion time (TI) linearly ranged from 50 ms to 6 s. The field of view (FOV) was 4 × 4 cm² with a matrix of 128 × 128. A series of multiple slices multiple echos (MSME) sequences was performed for T₂ measurements. The pulse sequence parameters were TR = 4 s, number of echoes = 8 with TE of 9, 18, 27, 36, 45, 54, 63, 72 ms; FOV = 4 × 4 cm² with a matrix of 128 × 128.

2.4. *Ex vivo* T₁ and T₂ measurements

All of the animal experiments were carried out in compliance with the institutional animal use and care protocols of the Georgia Institute of Technology and Emory University. Under anesthesia with 2–3% inhalant isoflurane, 9–10 week old male Fisher 344 rats were injected with 0.25 mmol Gd kg⁻¹ body weight of either the Gd-nanocarrier (*n* = 3) or gadodiamide (*n* = 3) intravenously (IV) in the tail vein using a 24G catheter. Blood samples were withdrawn orbitally once before injection and at 5, 35, 60, 180, 240 and 300 min after injection and transferred to heparinized blood tubes. Plasma was collected by centrifugation at 2000 rpm. The plasma T₁ and T₂ values were measured immediately as described above on the 9.4 T Bruker Biospin MR system.

2.5. 9L glioma cell culture

9L glioma cell line was maintained in MEM/EBSS medium supplemented with 10% fetal bovine serum and 0.05 mg ml⁻¹ gentamicin. Cells were passaged by trypsinization and washed with growth medium. Prior to implantation, cells were resuspended in serum-free Leibovitz's L-15 medium to a concentration of 2 × 10⁸ cells ml⁻¹.

2.6. Tumor inoculation

A rat glioma model was established by surgically implanting 2 × 10⁶ 9L glioma cells into the frontal lobe of 9–10 week old male Fisher 344 rats. All procedures were conducted under a protocol approved by the Institutional Animal Care and Use Committee (IACUC) at Georgia Institute of Technology. During surgery, anesthesia was maintained through the administration of 2–3% inhalant isoflurane. The incision site was shaved and the animal mounted in a stereotaxic frame. The scalp was opened to expose the skull, and a burr hole was drilled 2 mm anterior and 2 mm lateral to the bregma. 2 × 10⁶

9L glioma cells in 10 μl of Leibovitz's L-15 medium were slowly injected into the frontal lobe through a 21-gauge needle at a depth of 3 mm below the brain surface. The burr hole was then sealed with bone wax, and the scalp was sutured closed. Animals received 5 ml Lactated Ringer's solution through intraperitoneal (IP) injection and a subcutaneous injection of 0.5% marcaine at the wound site. Flunixin meglumine (2.5 mg kg⁻¹) was administered through an intramuscular injection to alleviate pain as needed.

2.7. *In vivo* images

All MRI image data were acquired on the 9.4 T Bruker system. A volume coil (72 mm inner diameter) and an inductively coupled surface coil (20 mm diameter) for signal built saddle volume coil was employed. High resolution angiograms of the rat brain ($n = 1$) were obtained before and 15 min after IV injection of the Gd-nanocarrier (at a dose of 0.25 mmol Gd kg⁻¹ b.w.) using a T_2^* -weighted 3D FLASH sequence with the following parameters: TR/TE = 50/15 ms, flip angle = 30°, matrix = 512 × 384 × 32, FOV = 4 × 3 × 0.5 cm³, and 8 averages (scan time = 81 min) for high resolution brain angiography. This resulted in an in-plane spatial resolution of 78 μm and a slice thickness of 156 μm .

The intratumoral extravascular accumulation of the nanocarrier was monitored by employing a 3D FLASH sequence with shorter scan time (and lower spatial resolution) than the high resolution angiograms with the following parameters: TR/TE = 50/15 ms, flip angle = 30°, matrix = 256 × 256 × 32, FOV = 4 × 3 × 0.75 cm³, and 2 averages (scan time = 13 min). This resulted in a spatial resolution of 156 μm × 117 μm × 234 μm . Two groups of animals were monitored for a period of three days after injection of 0.25 mmol Gd kg⁻¹ b.w. of the nanocarrier (group A; $n = 3$) and injection of a saline solution at equal volume to the nanocarrier (group B; $n = 3$). Imaging was performed pre-injection and 5 min, 1 day and 3 days post-injection. Care was taken to maintain similar positioning of the animal for pre- and post-contrast images. After each 3D imaging session, a T_2^* -weighted 2D map was obtained using a multi-gradient echo (MGE) sequence with the following parameters: TR/TE = 500/3 ms, number of echoes = 12, matrix = 128 × 128, FOV = 3.4 × 3.4 cm², and 8 averages (scan time = 9 min). At day 3 post-injection, the animals were euthanized immediately after completion of the last imaging session and histological analysis was performed as described below.

2.8. Immunohistochemistry and histological evaluation of explanted tumors

Upon completion of the imaging study, the animals were anesthetized with ketamine (1 mg kg⁻¹) and xylazine (0.17 mg kg⁻¹), transcardially perfused with 4% paraformaldehyde, the tumors were retrieved, and stored in 4% paraformaldehyde. The tumors were transferred from 4% paraformaldehyde to 30% sucrose and allowed to incubate for 48–72 h. Serial coronal cryostat (Leica CM 300, Leica, Bannockburn, IL) sections of 16 μm thickness were made and mounted onto glass slides. Care was taken to obtain brain

sections with the same orientation as that of the MR images. To visualize the tumor microvasculature, the tissue slices were immunohistochemically stained with RECA-1, a cell surface antigen which is expressed by all rat endothelial cells. After three washes in PBS for 10 min each, the sections were incubated in 4% goat serum and 0.5% Triton X-100 for 1 h. Upon adding the primary antibody (1:250 dilution) in 4% goat serum and 0.5% Triton X-100, the sections were incubated at 4 °C overnight. After washing the sections three times with PBS, the secondary antibody (1:220 dilution), Alexa Fluor 488 goat anti-mouse IgG, was added and allowed to incubate for 1 h. The sections were washed three times with PBS, incubated with DAPI (nuclear stain) for 15 min followed by three washes with PBS and covered with glass coverslips. The tumor sections were imaged at 20× on the Nikon Eclipse 80i upright microscope using a Microfire CCD camera (Optronics, Golate, CA) that interfaced with the Neurolucida software (MicroBrightField Bioscience, Williston, VT) to obtain a 2D montage of the entire brain tissue section.

2.9. Data and statistical analysis

The plasma T_1 and T_2 values measured *ex vivo* (figure 2) and the T_2^* values obtained from *in vivo* 2D mapping (figure 5) are expressed as mean ± standard deviation. To determine the significance of the relaxation times among the various animal groups at different time points, an unpaired *t* test analysis was performed. A *p*-value less than 0.05 was used to confirm significant differences at the 95% confidence level. The analysis was performed using the Minitab software.

3. Results and discussion

3.1. *In vitro* characterization of the Gd-nanocarrier

The liposomal Gd-nanocarrier contained 150 mM lipids and 87 mM Gd, 100% of Gd being encapsulated within the liposomes. The average diameter of the Gd-nanocarrier was 98 nm (standard deviation = 9 nm) as determined by dynamic light scattering, a size known to prevent renal clearance while allowing extravasation. The 600 mOsm kg⁻¹ water osmolality of the formulation allowed intravenous injection, since the liposomal walls can sustain the osmotic pressures expected to occur in isotonic environments. Indeed, *in vitro* leakage experiment against isotonic phosphate buffered saline exhibited very low leakage of the encapsulated Gd (less than 6% of the initial payload) over a period of three days.

The r_1 and r_2 relaxivities of the Gd-nanocarrier at 25 °C and 9.4 T were 0.65 and 20.7 s⁻¹ mM⁻¹, respectively (figure 1). At the high magnetic field of 9.4 T, the r_2/r_1 ratio of the Gd-nanocarrier substantially increased, which is expected since the r_2/r_1 ratio usually increases with increasing resonance frequencies (Strijkers *et al* 2005). Previous studies have measured the r_2 relaxivity of liposomal Gd to be around 1 s⁻¹ mM⁻¹ on 0.47 T magnets, a value significantly smaller than the one measured on the 9.4 T system. This high r_2 value allowed us to use the Gd-nanocarrier in the *in vivo* imaging studies as a T_2 -shortening agent.

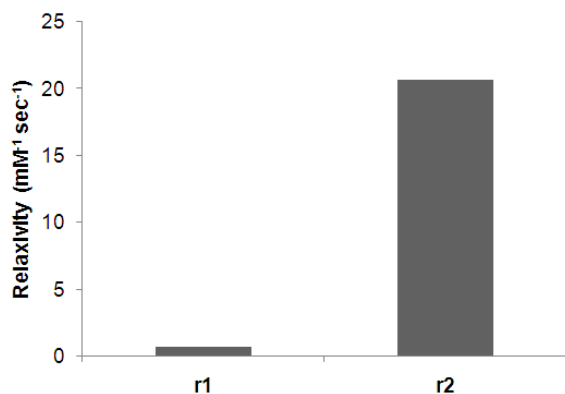


Figure 1. *In vitro* r_1 and r_2 relaxivities of the Gd-nanocarrier measured on 9.4 T and 25 °C.

3.2. *Ex vivo* plasma T_1 and T_2 measurements

Figure 2(a) shows the changes in plasma T_1 relaxation time measured at 9.4 T following administration of Gd-nanocarrier and gadodiamide. At $t = 5$ min after administration of the nanocarrier, a sharp decrease of the T_1 value from the pre-injection value of 2500 ms to the post-injection value of 570 ms was observed. Due to the prolonged blood residence time of the nanocarrier (Lasic and Martin 1995), the plasma T_1 value remained at low values of about 650 ms for the rest of the duration of the experiment. While we did not attempt to measure the blood half life ($t_{1/2}$) in this study, we have shown that liposomes of similar size and lipid composition as the Gd-nanocarrier have a $t_{1/2}$ of about 18 h in Fisher rats (McNeeley *et al* 2007). In a previous study (Ayyagari *et al* 2006), we observed that the post-injection T_1 values were about 180 ms measured at 0.47 T upon administration of the Gd-nanocarrier at a dose similar to the one used in the current study. This difference is expected since higher resonance frequencies (or magnetic strength such as that used in the current study) produce longer T_1 values. Following administration of (non-liposomal) gadodiamide, the plasma T_1 value decreased to about 450 ms at 5 min post-injection. The rapid clearance of

the agent from blood circulation resulted in a rapid increase of the T_1 value reaching the pre-injection value within 2 h after administration. Similarly, administration of the Gd-nanocarrier resulted in a rapid drop of the plasma T_2 value from the pre-injected value of 113 ms to the post-injection value of about 16 msec which remained at these low values for the rest of the duration of the experiment (figure 2(b)). Such low plasma T_2 values suggest that the gadolinium-based contrast agent being packaged in the nanocarrier displays improved magnetic properties when used as a T_2 -shortening agent at the high magnetic field of 9.4 T. Upon injection of (non-liposomal) gadodiamide, the plasma T_2 value dropped to 59 ms at 5 min post-injection and then rapidly returned to the pre-injection value.

3.3. MR angiograms

Figure 3 shows high resolution coronal T_2^* -weighted images obtained using the 9.4 T MRI before and after administration of the Gd-nanocarrier. It should be noted that the scanning parameters in the pre- and post-contrast images were identical. In the pre-contrast image (figure 3(a)), few blood vessels (appear as black dots) of the vasculature of the cerebral cortex can be seen in the healthy tissue or in the cancerous lesion located in the front of the right hemisphere (as indicated by the arrow). The prolonged blood circulation of the Gd-nanocarrier allowed negatively enhanced signal for long time increasing scanning times and the time window for image acquisition (subsequently lowering the signal to noise ratio). Administration of the nanoscale agent allowed clear visualization of the cerebral vasculature (figure 3(b)). Importantly, details of the glioma vasculature were revealed in the post-contrast image. The tumor lesion consisted of a spherical and an envelope-shaped part (as indicated in figure 3(b)). The sphere part (where originally inoculation of the cancer cells occurred) was characterized by a highly vascularized peripheral rim which is usually associated with high levels of angiogenic and permeability factors resulting in neoangiogenesis (Damert *et al* 1997, Takano *et al* 1996) and an

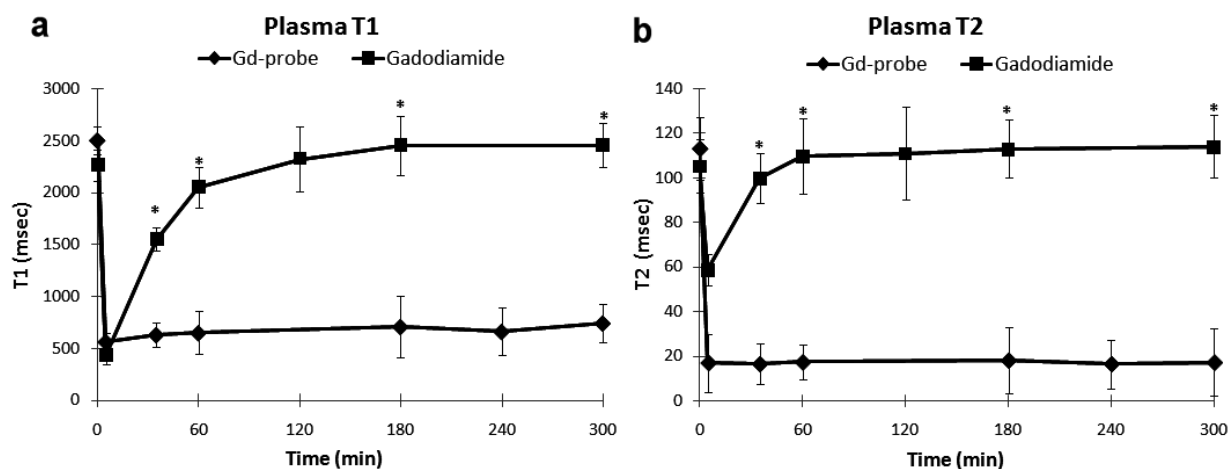


Figure 2. Plasma relaxation time (a) T_1 and (b) T_2 measured *ex vivo* on 9.4 T after administration of the liposomal Gd-nanocarrier ($n = 3$) and gadodiamide ($n = 3$) at a dose of 0.25 mmol Gd kg⁻¹. The * indicates significant statistical difference ($p < 0.05$) between the Gd-nanocarrier and gadodiamide.

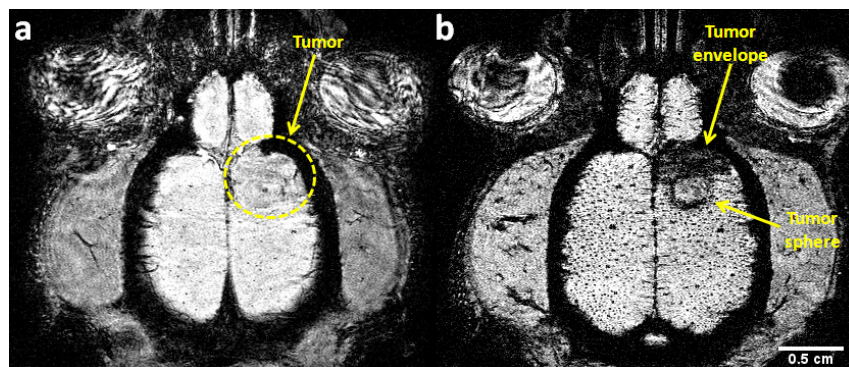


Figure 3. High resolution ($78\ \mu\text{m}$ in-plane resolution) coronal T_2^* -weighted images of rat brain on a 9.4 T MRI. (a) In the pre-contrast image, minor vasculature enhancement was seen in the normal cerebral tissue and tumor (arrow). (b) Administration of $0.25\ \text{mmol Gd kg}^{-1}$ of the nanocarrier allowed clear visualization of the vasculature of the normal cerebral tissue. The post-contrast image revealed a spherical part of the tumor lesion with highly vascularized rim and a less vascularized inner core and a very well-vascularized envelope-shaped part of the lesion (scale bar is 0.5 cm).

(This figure is in colour only in the electronic version)

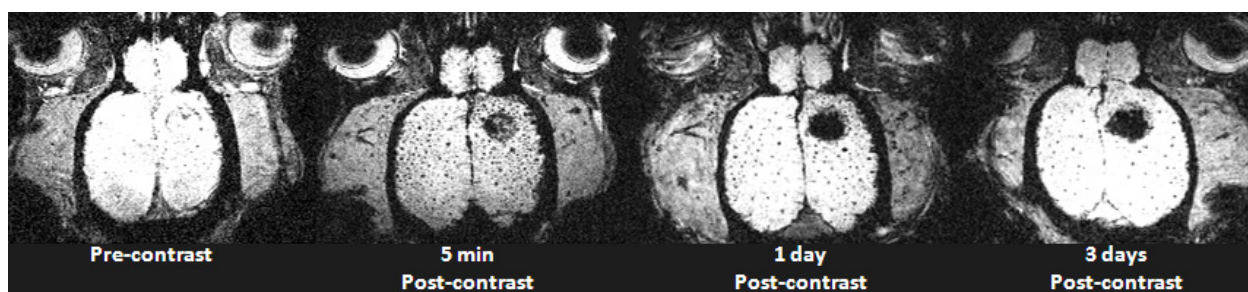


Figure 4. Coronal T_2^* -weighted images of rat brain with spatial resolution of $156\ \mu\text{m} \times 117\ \mu\text{m} \times 234\ \mu\text{m}$ obtained before and 5 min, 1 day and 3 days after administration of the Gd-nanocarrier at a dose of $0.25\ \text{mmol Gd kg}^{-1}$ on a 9.4 T MRI.

inner core with less vascularization. The entire envelope (the other portion of the tumor) appeared highly vascularized. In previous studies (McNeeley *et al* 2007), we have observed in many cases a similar pattern where the glioma grows initially as a sphere and then grows towards the front of the lobe most likely due to less restriction (e.g. pressure).

3.4. Intratumoral visualization of the nanocarrier

The Gd-nanocarrier was tested in adult male rats using an orthotopic brain tumor model developed by inoculation of 9 L glioma cells. By utilizing a fast imaging protocol (with a duration of 13 min), we were able to obtain images of the brain with a spatial resolution of $156\ \mu\text{m} \times 117\ \mu\text{m} \times 234\ \mu\text{m}$. Figure 4 shows brain images of the same animal before and 5 min, 1 day and 3 days after injection of the Gd-nanocarrier. High density vasculature in normal and tumor tissue can be visualized immediately after injection. Over the time course of three days, the tumor exhibited increasing negative enhancement whereas the negative enhancement of the blood vessels in normal tissue was disappearing. This is consistent with clearance of the nanocarrier from circulation while accumulation of the agent within the intratumoral extravascular space via extravasation through the tumor's leaky

vasculature was increasing. It should be noted that the vasculature of normal brain with intact BBB is impermeable to the nanocarrier. In previous reports from our lab (McNeeley *et al* 2007), we have shown that the half life ($t_{1/2}$) of liposomes in rat blood circulation is about 18 h and that less than 10% of the nanocarrier remained in circulation at three days post-injection. To verify the low levels of the nanocarrier in blood, a blood sample was obtained and measured *ex vivo* using the 9.4 T MRI (similar to the measurements in section 3.2). The plasma T_2 value at 3 days post-contrast was 108 ms which is close to the pre-contrast values. A comparison of the enhancement of normal brain vasculature in the pre-contrast and in the 3-day post-contrast image (figure 4) also supports the fact that low levels of the nanocarrier remained in circulation 3 days after administration. This allowed clear visualization of the extravascular accumulation of the nanocarrier since minor interfering signal was obtained from the blood side. The time course of the increase of tumor enhancement is consistent with previous reports in which biodistribution studies showed that the liposome intratumoral accumulation in rat brain tumors (McNeeley *et al* 2007) and mouse breast tumors (Kirpotin *et al* 2006) peaks at 24–48 h after injection.

Gadodiamide chelates have been extensively employed to perform dynamic contrast-enhanced MRI to evaluate tumor

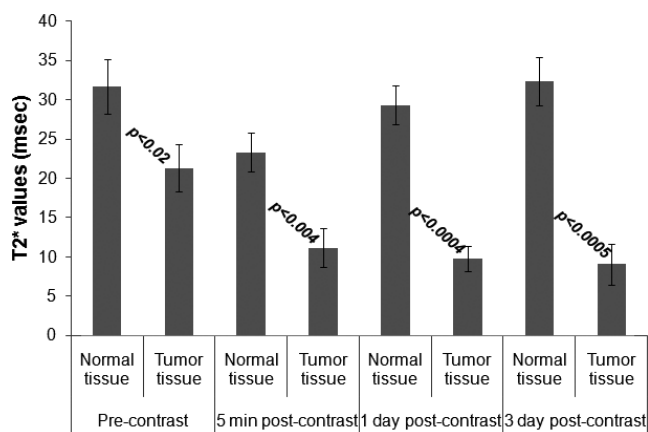


Figure 5. Comparison of T_2^* values of normal brain and tumor obtained via T_2^* -weighted 2D maps over the period of 3 days before and after administration of $0.25 \text{ mmol Gd kg}^{-1}$ of the nanocarrier in rats ($n = 3$).

vasculature leakiness in animals and patients (Brix *et al* 2004, Furman-Haran and Degani 2002, Leach 2001, Oshida *et al* 2005, Sardanelli *et al* 2005, Teifke *et al* 2006). These studies show that the temporal intratumoral uptake of the contrast agent displays a fast wash-in–wash-out profile indicating that the agent leaks out of the blood vessel into the tumor extravascular space and returns back to the blood in short times. This is not surprising since the transport of molecules (such as gadodiamide) is governed by passive diffusion, whereas extravasation of nanoparticles is governed by convective terms and therefore once a liposome extravasates it is generally difficult to return back to blood stream (Jain 1999). While it is difficult to directly determine whether the Gd chelate was intraliposomal when the nanocarrier was deposited in the tumor extravascular space, it is reasonable to assume that the chelate would quickly return to the blood if it were not encapsulated within the liposome.

To better realize the intratumoral accumulation of the nanocarrier, we performed T_2^* mapping and subsequently quantified the T_2^* values of the normal and the tumor tissue. Figure 5 summarizes these findings. Even before administration of the nanocarrier, the tumor tissue displayed significantly lower T_2^* values than normal brain consistent with cancer-related neovascularization resulting in higher density of vasculature in the tumor comparing to normal brain. Immediately after administration of the nanocarrier, the T_2^* values of both normal and tumor tissue dropped significantly. While the values of normal brain reached its pre-contrast values in 3 days after injection, the T_2^* values remained low displaying a statistically significant difference when compared to the pre-contrast values of the tumor tissue ($p < 0.001$). This suggests that the nanocarrier was cleared from blood circulation while accumulated in the extravascular space of the tumor.

In the past, nanoscale liposomal contrast agents encapsulating Gd with prolonged blood circulation were used for blood pool imaging (Ghaghada *et al* 2007, Erdogan *et al* 2008, 2006, Torchilin 1994, Krauze *et al* 2006, Weissing *et al* 2000) but not for detecting extravascular deposition in tumors. Other

macromolecular gadolinium-based agents (Daldrup *et al* 1998) and iron oxide nanoparticles (USIOP) (Turetschek *et al* 2001b, 2001a) have been employed to evaluate tumor vascular permeability. These agents and method of use however, failed to transparently characterize the tumor vascular permeability to nanoparticles due to persistent intravascular signal and/or inadequate extravascular signal. The primary explanation for these results is that the short duration of the imaging sessions (less than 1 h) used in those studies did not allow enough time for extravasation of large quantities of the nanoscale contrast agents to yield adequate signal. Indeed it has been established that the intratumoral, extravascular accumulation of long-circulating nanoscale agents peaks at about 48 h (Kirpotin *et al* 2006). Though a liposomal-based nanocarrier enabled evaluation of vascular permeability in this study, we hypothesize that such evaluation would be possible with other long-circulating nanoscale contrast agents as well. However, liposomal nanocarriers can serve as multifunctional agents since they can carry combinations of drugs and contrast agents and can conveniently be modified for active targeting (Zalipsky 1993).

3.5. Histological analysis

Histological analysis of tumors was performed on animals euthanized three days after administration of the rhodamine-tagged Gd-nanocarrier (immediately after completion of the last imaging session). Fluorescent microscopy of brain tissue section verified the intratumoral extravascular deposition of the nanocarrier. The tumor was characterized by a highly vascularized peripheral rim and an internal core with a lower vascularization (figure 6(a)), consistent with earlier reports (Marzola *et al* 2005, McNeeley *et al* 2007). In the same histological slice (figure 6(b)) the extravasated nanocarrier was observed to localize within the lesion (not in normal brain) exhibiting a patchy distribution. The typical intratumoral microdistribution of PEGylated liposomes is predominantly at the tumor (Kirpotin *et al* 2006, Huang *et al* 1992, Yuan *et al* 1994), which is usually associated with high levels of angiogenic and permeability factors resulting in neoangiogenesis (Damert *et al* 1997, Takano *et al* 1996). This is consistent with our histological observations.

4. Conclusions

In this work, we demonstrated the ability to track non-invasively the fate of a systemically-administered nanocarrier. The nanocarrier consists of a 100 nm scale long-circulating liposomal agent encapsulating gadolinium of similar composition and particle size as the clinically used liposomal chemotherapy (Lasic and Papahadjopoulos 1995). While gadolinium is traditionally used as a T_1 -shortening contrast agent under the currently used magnetic fields in the clinic (1.5–3 T), the Gd-containing nanocarrier behaved as a potent T_2 -shortening agent on a 9.4 T MRI system. The significant T_2 shortening effect of the nanocarrier and the method of use allowed detection of the intratumoral, extravascular accumulation of the nanocarrier in a rat brain tumor model using a 9.4 T MRI system. It would be expected that a long-circulating

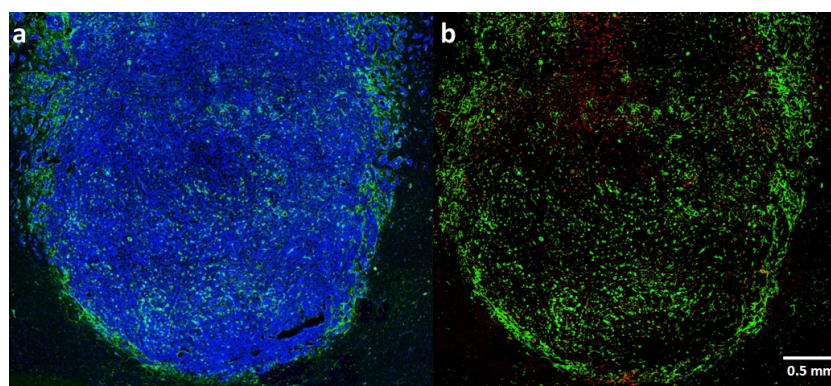


Figure 6. Microdistribution of the nanocarrier in the brain tumor lesion (the MR images of the same animal are shown in figure 4) 72 h after IV injection of rhodamine-tagged Gd-nanocarrier using fluorescent microscopy at 20 \times magnification. (a) Immunohistochemical microvascular staining was achieved by staining with RECA-1, a cell surface antigen which is expressed by all rat endothelial cells (appeared as green) revealing a highly vascularized peripheral rim and a less vascularized inner core (DAPI was used as a nuclear stain; appeared as blue); (b) In the same histological slice, the liposomes (appeared as red) displayed a patchy distribution (scale bar is 0.5 mm).

agent would produce undistinguishable extravascular and intravascular signal making determination of the degree of vascular permeability unfeasible. This is the case for the first 24 h after injection since the intravascular levels of the agent are still high. As the concentration of the nanocarrier in the blood decreased, its extravascular accumulation in the tumor increased resulting in adequate negative enhancement without interference from the blood for detection. This allowed the evaluation of the nanocarrier uptake by a brain tumor 3 days post-injection. The visualization of the extravascular accumulation of the nanocarrier and at the same time invisibility of the vasculature makes MR imaging an attractive non-invasive method. Such an *a priori* determination of the extent of tumor susceptibility to nanocarrier-based chemotherapy would therefore facilitate personalized therapy, and spare potential non-responders from the rigors of a chemotherapy regimen. However, human cancer as a disease is much more heterogeneous than experimental tumor models in terms of both tumors and hosts. The current study demonstrated the feasibility of tracking the intratumoral deposition of the Gd-loaded nanocarrier on a single tumor model, and further testing of imaging followed by treatment in more tumor models is required to fully assess the clinical value of this approach. Recently, we have fabricated a liposomal nanocarrier co-encapsulating Gd and doxorubicin (data not shown). Future studies will be performed with the nanocarrier co-encapsulating the contrast agent and the drug, and determine that indeed a rationally determined treatment regime would significantly enhance therapeutic efficacy of the chemotherapeutic nanocarriers. In addition, surgical units are increasingly co-locating MRI units to assist in surgical planning. Imaging of tumor border and location using MRI could also serve as a useful surgical planning tool for tumor border mapping and resection.

Acknowledgments

This work was funded by the National Science Foundation (NSF), Bioengineering and Environmental Systems (0401627) and the Georgia Cancer Coalition (to RVB). The authors would like to acknowledge Ketan Ghaghada and Kathleen McNeely

for useful discussions. We also thank Dr Gang Bao for helping us with measurements using the NMR Minispec.

References

- Arnold R D, Mager D E, Slack J E and Straubinger R M 2005 Effect of repetitive administration of doxorubicin-containing liposomes on plasma pharmacokinetics and drug biodistribution in a rat brain tumor model *Clin. Cancer Res.* **11** 8856–65
- Ayyagari A L, Zhang X, Ghaghada K B, Annapragada A, Hu X and Bellamkonda R V 2006 Long-circulating liposomal contrast agents for magnetic resonance imaging *Magn. Reson. Med.* **55** 1023–9
- Barker F G 2nd, Chang S M, Gutin P H, Malec M K, McDermott M W, Prados M D and Wilson C B 1998 Survival and functional status after resection of recurrent glioblastoma multiforme *Neurosurgery* **42** 709–20 discussion 20–3
- Black K L and Pikul B K 1999 Gliomas—past, present, and future *Clin. Neurosurg.* **45** 160–3
- Brix G, Kiessling F, Lucht R, Darai S, Wasser K, Delorme S and Griebel J 2004 Microcirculation and microvasculature in breast tumors: pharmacokinetic analysis of dynamic MR image series *Magn. Reson. Med.* **52** 420–9
- Daldrup H, Shames D M, Wendland M, Okuhata Y, Link T M, Rosenau W, Lu Y and Brasch R C 1998 Correlation of dynamic contrast-enhanced MR imaging with histologic tumor grade: comparison of macromolecular and small-molecular contrast media *AJR Am. J. Roentgenol.* **171** 941–9
- Damert A, Machein M, Breier G, Fujita M Q, Hanahan D, Risau W and Plate K H 1997 Up-regulation of vascular endothelial growth factor expression in a rat glioma is conferred by two distinct hypoxia-driven mechanisms *Cancer Res.* **57** 3860–4
- Erdogan S, Medarova Z O, Roby A, Moore A and Torchilin V P 2008 Enhanced tumor MR imaging with gadolinium-loaded polychelating polymer-containing tumor-targeted liposomes *J. Magn. Reson. Imaging* **27** 574–80
- Erdogan S, Roby A, Sawant R, Hurley J and Torchilin V P 2006 Gadolinium-loaded polychelating polymer-containing cancer cell-specific immunoliposomes *J. Liposome Res.* **16** 45–55
- Ferrari M 2005 Cancer nanotechnology: opportunities and challenges *Nat. Rev. Cancer* **5** 161–71
- Fine H A, Dear K B, Loeffler J S, Black P M and Canellos G P 1993 Meta-analysis of radiation therapy with and without adjuvant chemotherapy for malignant gliomas in adults *Cancer* **71** 2585–97

- Fukumura D and Jain R K 2007 Tumor microenvironment abnormalities: causes, consequences, and strategies to normalize *J. Cell. Biochem.* **101** 937–49
- Furman-Haran E and Degani H 2002 Parametric analysis of breast MRI *J. Comput. Assist. Tomogr.* **26** 376–86
- Ghaghada K B, Bockhorst K H, Mukundan S Jr, Annapragada A V and Narayana P A 2007 High-resolution vascular imaging of the rat spine using liposomal blood pool MR agent *AJNR Am. J. Neuroradiol* **28** 48–53
- Heath J R and Davis M E 2007 Nanotechnology and Cancer *Annu. Rev. Med.* **59** 251–65
- Hobbs S K, Monsky W L, Yuan F, Roberts W G, Griffith L, Torchilin V P and Jain R K 1998 Regulation of transport pathways in tumor vessels: role of tumor type and microenvironment *Proc. Natl Acad. Sci. USA* **95** 4607–12
- Hong S, Leroueil P R, Majoros I J, Orr B G, Baker J R Jr and Banaszak Holl M M 2007 The binding avidity of a nanoparticle-based multivalent targeted drug delivery platform *Chem. Biol.* **14** 107–15
- Huang S K, Lee K D, Hong K, Friend D S and Papahadjopoulos D 1992 Microscopic localization of sterically stabilized liposomes in colon carcinoma-bearing mice *Cancer Res.* **52** 5135–43
- Jain R K 1994 Barriers to drug delivery in solid tumors *Sci. Am.* **271** 58–65
- Jain R K 1999 Transport of molecules, particles, and cells in solid tumors *Annu. Rev. Biomed. Eng.* **1** 241–63
- Jain R K 2001 Delivery of molecular and cellular medicine to solid tumors *Adv. Drug Deliv. Rev.* **46** 149–68
- Jain R K 2005 Normalization of tumor vasculature: an emerging concept in antiangiogenic therapy *Science* **307** 58–62
- Kim D H and Rossi J J 2007 Strategies for silencing human disease using RNA interference *Nat. Rev. Genet.* **8** 173–84
- Kirpotin D B, Drummond D C, Shao Y, Shalaby M R, Hong K, Nielsen U B, Marks J D, Benz C C and Park J W 2006 Antibody targeting of long-circulating lipidic nanoparticles does not increase tumor localization but does increase internalization in animal models *Cancer Res.* **66** 6732–40
- Koning G A and Krijger G C 2007 Targeted multifunctional lipid-based nanocarriers for image-guided drug delivery *Anticancer Agents Med. Chem.* **7** 425–40
- Koukourakis M I, Koukouraki S, Fezoulidis I, Kelekis N, Kyrias G, Archimandritis S and Karkavitsas N 2000 High intratumoural accumulation of stealth liposomal doxorubicin (Caelyx) in glioblastomas and in metastatic brain tumours *Br. J. Cancer* **83** 1281–6
- Krauze M T, Forsayeth J, Park J W and Bankiewicz K S 2006 Real-time imaging and quantification of brain delivery of liposomes *Pharm. Res.* **23** 2493–504
- Lasic D and Martin F 1995 *Stealth Liposomes* (Boca Raton, FL: CRC Press)
- Lasic D D and Papahadjopoulos D 1995 Liposomes revisited *Science* **267** 1275–6
- Leach M O 2001 Application of magnetic resonance imaging to angiogenesis in breast cancer *Breast Cancer Res. Treat.* **3** 22–7
- Maeda H, Wu J, Sawa T, Matsumura Y and Hori K 2000 Tumor vascular permeability and the EPR effect in macromolecular therapeutics: a review *J. Control. Release* **65** 271–84
- Marzola P *et al* 2005 Effect of tamoxifen in an experimental model of breast tumor studied by dynamic contrast-enhanced magnetic resonance imaging and different contrast agents *Invest. Radiol.* **40** 421–9
- McNeeley K M, Annapragada A and Bellamkonda R V 2007 Decreased circulation time offsets increased efficacy of PEGylated nanocarriers targeting folate receptors of glioma *Nanotechnology* **18** 385101
- Mitra A, Nan A, Line B R and Ghandehari H 2006 Nanocarriers for nuclear imaging and radiotherapy of cancer *Curr. Pharm. Des.* **12** 4729–49
- Oshida K, Nagashima T, Ueda T, Yagata H, Tanabe N, Nakano S, Nikaidou T, Funatsu H, Hashimoto H and Miyazaki M 2005 Pharmacokinetic analysis of ductal carcinoma in situ of the breast using dynamic MR mammography *Eur. Radiol.* **15** 1353–60
- Sardanelli F, Iozzelli A, Fausto A, Carriero A and Kirchin M A 2005 Gadobenate dimeglumine-enhanced MR imaging breast vascular maps: association between invasive cancer and ipsilateral increased vascularity *Radiology* **235** 791–7
- Saul J M, Annapragada A V and Bellamkonda R V 2006 A dual-ligand approach for enhancing targeting selectivity of therapeutic nanocarriers *J. Control. Release* **114** 277–87
- Schiffelers R M, Ansari A, Xu J, Zhou Q, Tang Q, Storm G, Molema G, Lu P Y, Scaria P V and Woodle M C 2004 Cancer siRNA therapy by tumor selective delivery with ligand-targeted sterically stabilized nanoparticle *Nucleic Acids Res.* **32** e149
- Service R F 2005 Materials and biology. Nanotechnology takes aim at cancer *Science* **310** 1132–4
- Strijkers G J, Mulder W J, van Heeswijk R B, Frederik P M, Bomans P, Magusin P C and Nicolay K 2005 Relaxivity of liposomal paramagnetic MRI contrast agents *Magn. Reson. Mater. Phys. Biol. Med.* **18** 186–92
- Takano S, Yoshii Y, Kondo S, Suzuki H, Maruno T, Shirai S and Nose T 1996 Concentration of vascular endothelial growth factor in the serum and tumor tissue of brain tumor patients *Cancer Res.* **56** 2185–90
- Teifke A, Behr O, Schmidt M, Victor A, Vomweg T W, Thelen M and Lehr H A 2006 Dynamic MR imaging of breast lesions: correlation with microvessel distribution pattern and histologic characteristics of prognosis *Radiology* **239** 351–60
- Torchilin V P 1994 Immunoliposomes and PEGylated immunoliposomes: possible use for targeted delivery of imaging agents *Immunomethods* **4** 244–58
- Torchilin V P 2006 Multifunctional nanocarriers *Adv. Drug Deliv. Rev.* **58** 1532–55
- Turetschek K, Huber S, Floyd E, Helbich T, Roberts T P, Shames D M, Tarlo K S, Wendland M F and Brasch R C 2001a MR imaging characterization of microvessels in experimental breast tumors by using a particulate contrast agent with histopathologic correlation *Radiology* **218** 562–9
- Turetschek K, Roberts T P, Floyd E, Preda A, Novikov V, Shames D M, Carter W O and Brasch R C 2001b Tumor microvascular characterization using ultrasmall superparamagnetic iron oxide particles (USPIO) in an experimental breast cancer model *J. Magn. Reson. Imaging* **13** 882–8
- van de Wiele P, Dierckx R, Scopinaro F, Waterhouse R, Annovazzi A, Kolindou A and Signore A 2002 Nuclear medicine imaging for prediction or early assessment of response to chemotherapy in patients suffering from breast carcinoma *Breast Cancer Res. Treat.* **72** 279–86
- Weissing V, Babich J and Torchilin V 2000 Long-circulating gadolinium loaded liposomes: potential use for magnetic resonance imaging of the blood pool *Colloids Surf. B* **18** 293–9
- Yuan F, Chen Y, Dellian M, Safabakhsh N, Ferrara N and Jain R K 1996 Time-dependent vascular regression and permeability changes in established human tumor xenografts induced by an anti-vascular endothelial growth factor/vascular permeability factor antibody *Proc. Natl Acad. Sci. USA* **93** 14765–70
- Yuan F, Leunig M, Huang S K, Berk D A, Papahadjopoulos D and Jain R K 1994 Microvascular permeability and interstitial penetration of sterically stabilized (stealth) liposomes in a human tumor xenograft *Cancer Res.* **54** 3352–6
- Zalipsky S 1993 Synthesis of an end-group functionalized polyethylene glycol–lipid conjugate for preparation of polymer-grafted liposomes *Bioconjug. Chem.* **4** 296–9